Influence of Positioning-Induced Changes in Pelvic Angle on Occupant Kinematics and Injury Risk in Human Body Models during Frontal Loading

Sonja Fitterer, Desiree Kofler, Jingwen Hu, Felix Ressi, Chirag Shah, Corina Klug

Abstract Occupant positioning is a relevant aspect of Human Body Model (HBM) crash simulations, as postural differences may influence kinematics and injury prediction. This study investigated the effect of positioning workflow on pelvic angle and crash response in VIVA+ 50M v2.0.1 and HBM-Connect 50M v2.5 compared with Total Human Model for Safety (THUMS) as reference. Both HBMs were positioned to landmark targets derived from a morphed and positioned THUMS midsize male HBM, seated in a Toyota RAV4 driver FE environment. Two sequential two-step positioning workflows were applied, and frontal crash simulations were performed with all HBMs at 32 km/h and 61 km/h. The VIVA+ and HBM Connect achieved small deviations from the THUMS target landmark coordinates. However, workflow dependent differences in pelvic angle remained, particularly for HBM Connect 50M, whereas VIVA+ 50M remained closer to the THUMS reference posture. These differences were associated with changes in lap belt loading, femur and tibia forces, thoracic response, and selected head injury metrics. The results show that close agreement in external landmark coordinates does not necessarily result in biomechanically equivalent posture. In addition to landmark accuracy, pelvic angle should therefore be considered when evaluating HBM positioning procedures and interpreting inter-model differences in frontal crash simulations.

Keywords Human body models, Injury risk assessment, Pelvic angle, Positioning procedures

I. INTRODUCTION

The advancement of virtual testing methodologies using Finite Element Human Body Models (HBMs) represents a paradigm shift in occupant safety assessment. Recent initiatives by consumer protection organisations, including the European New Car Assessment Programme (Euro NCAP), have established qualification procedures for HBMs to support standardised virtual testing and the planned integration of HBM simulations into consumer safety assessments [1–2]. The transition towards virtual testing promises enhanced injury prediction capabilities and the evaluation of diverse occupant populations across loading conditions that are impractical or impossible to assess with physical dummies alone. However, the integration of HBMs into regulatory and consumer testing frameworks requires rigorous standardisation of modelling practices, particularly concerning occupant positioning procedures [3].

Human body model positioning is a critical prerequisite for valid crash simulations, as initial posture directly influences occupant kinematics and injury outcomes. Several positioning methodologies have been developed, ranging from simulation-based approaches that apply forces or prescribed displacements to iteratively adjust model posture, to interpolation-based methods using radial basis functions or Laplacian transformations [3–5]. The PIPER positioning framework exemplifies physics-based positioning tools that enable reproducible landmark-based positioning of both Finite Element (FE) and multi-body models whilst accounting for anthropometric variations [3]. Despite these advances, positioning workflows remain largely model-specific and researcher-dependent, with limited consensus on optimal procedures. This lack of standardisation is particularly problematic given that Euro NCAP qualification procedures stipulate that any changes to HBM posture, except for extremity

Sonja Fitterer is a PhD student in Biomechanics (+43 316 87330367, s.fitterer@student.tugraz.at), D. Kofler is a Project Assistant, F. Ressi is a Senior Scientist and C. Klug is Associate Professor at the Vehicle Safety Institute of Graz University of Technology, Austria. Jingwen Hu is a Research Professor at the Biosciences Group of the University of Michigan Transportation Research Institute, USA. Chirag Shah is a Project Development Manager at Humanetics Innovative Solutions, USA.

adjustments, require full model re-qualification [1] underscoring the regulatory significance of positioning procedure consistency. Accumulated evidences demonstrate that occupant posture exerts substantial influence on crash injury prediction. Research assessing the sensitivity of thoracic injury risk criteria to HBM individualisation techniques, including spine alignment to Post Mortem Human Subject (PMHS) postures, and found that whilst mass scaling and morphing significantly influenced the prediction of Abbreviated Injury Scale (AIS) 3+ rib fractures, posture variations alone did not show statistically significant differences [6]. Conversely, studies investigating reclined occupant configurations have revealed that pelvic angle and spinal alignment profoundly affect pelvis-to-lap belt interaction and submarining risk [7–9]. It was demonstrated that pelvis orientation, influenced by seat friction and initial settling procedures, substantially alters pelvic kinematics and submarining outcomes in frontal crashes [7]. Moreover, previous research reported that during HBM positioning simulations, pelvis orientation and spinal alignment are determined by the biomechanical properties inherent to each model, suggesting that positioning workflows may interact with model-specific characteristics to produce divergent initial postures [10].
The sensitivity of injury predictions to pre-crash posture extends beyond pelvic orientation. Previous research found that arm and leg posture during braking manoeuvres influenced peak head excursion by up to 80 % variation in reactive HBMs, with arm positioning exhibiting a comparatively larger effect than leg posture [11].

A study investigating frontal impact simulations showed that variations in pre-impact posture can alter reaction forces, chest deflections, rib strain and fracture outcomes, even when the same HBM is used [12]. A related whole-body side-impact study further demonstrated that pre-impact spinal posture substantially affects reaction forces, deflections, strain histories and predicted fracture patterns [13]. Head and torso kinematics in active HBM braking simulations were found to be particularly sensitive to spinal alignment [14]. Furthermore, researchers identified occupant posture as the parameter with the greatest influence on overall injury risk in frontal collisions, among several pre-collision occupant parameters [15]. Similarly, finite element reconstructions of real-world frontal crashes have shown that variations in pre-crash occupant position can substantially influence predicted injury risks and injury metrics across multiple body regions [16]. Furthermore, variability in arm positioning exerted a greater influence on thoracic injury metrics in side impacts than modifications to restraint systems did [17]. Studies comparing slouched and nominal driving postures have documented relative differences in lumbar spine compression forces of up to 38% [18], while investigations into real-world crash heterogeneity indicate that variations in lower extremity posture produce the most pronounced effects on whole-body kinematic and kinetic responses across diverse crash scenarios [10].

These findings collectively underscore those subtle variations in initial occupant configuration, whether arising from positioning methodology, model-specific biomechanical properties, or real-world diversity, can propagate through simulations to produce meaningful differences in predicted injury outcome. Despite the recognised importance of posture, there exists a notable gap in the literature regarding the quantification of positioning-induced variability relative to inherent inter-model differences. Whilst comparative evaluations of HBMs have been conducted, these studies typically position models to match average PMHS configurations without systematically isolating the influence of positioning workflow choices [19]. For example, comparisons of the SAFER and VIVA+ 50F HBMs revealed large differences in lumbar spine forces and pelvis pitch during reclined frontal impacts, attributed in part to differences in initial pelvis angle and lumbar flexion [19]. However, it remains unclear whether these discrepancies stem primarily from intrinsic model architecture or from positioning-induced posture variations. Addressing this ambiguity is essential for interpreting inter-model comparison studies and for establishing whether standardised positioning protocols can reduce apparent model-to-model differences. Pelvic angle, defined by anatomical landmarks such as the anterior superior iliac spine (ASIS) and pubic symphysis, is a fundamental postural parameter in biomechanical analyses. Within automotive safety, pelvic orientation relative to the lap belt, affects load transfer pathways and the risk of submarining in frontal crashes [7–9]. Researchers developed statistical models to predict driver posture based on vehicle geometry and occupant anthropometry in a previous study. These models demonstrated that individual drivers exhibit systematic variations in pelvic orientation, torso recline, and limb positioning [20]. These posture prediction models have been employed to position HBMs in parametric crash simulations, yet the sensitivity of injury outcomes to pelvic angle variations arising from different positioning workflows has not been explicitly quantified.

The present study addresses this gap by systematically investigating how pelvic angle variations induced by different positioning workflows influence occupant kinematics and injury prediction in two contemporary HBMs, VIVA+ 50M v2.0.1 [21] and HBM-Connect 50M v2.5 [22]. It provides a first quantitative assessment of how positioning workflow choices propagate through crash simulations to affect injury predictions, both within individual HBMs and in comparisons between models. The study is therefore relevant to the development of standardised virtual testing protocols and to the interpretation of inter-model comparison studies.

II. METHODS

This study combined landmark based FE occupant positioning and frontal crash simulation to investigate how positioning-induced variations in pelvic angle influence occupant kinematics and injury risk prediction in HBMs. Two HBMs, positioned according to a Total Human Model for Safety (THUMS) midsize male model, were evaluated in a validated driving compartment model representing a Toyota RAV4 [23] under two standardised frontal load cases [24]. The crash pulse was based on a prediction model developed by [25].

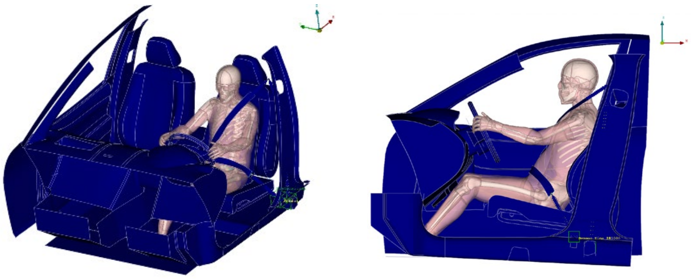

Fig. 1. Toyota RAV4 FE-Environment [23] with positioned THUMS.

By applying different positioning workflows to each HBM while keeping the vehicle, restraints, and crash pulses unchanged, the study isolated the effect of workflow dependent pelvic orientation on predicted responses.

Anatomical Landmarks and Target Posture Definition

Three male HBMs were considered in this study: the morphed THUMS v4.1 AM50 model as reference, and the VIVA+ 50M v2.0.1 and HBM-Connect 50M v2.5 models as the evaluated HBMs. All three models represent 50th percentile male occupants, thereby reducing the influence of gross anthropometric differences and allowing the study to focus on positioning-workflow effects and model-specific biomechanical response. The VIVA+ 50M model represents an average male occupant with a height of 1.753 m, BMI of 25 kg/m², and target age of 50 years [21]. Its reference anthropometry follows the average dummy targets from [26], which are based on the U.S. National Health and Nutrition Examination Survey 1971–1974 [27]. The HBM-Connect 50M model represents a 50th percentile adult male anthropometry based on the UMTRI statistical representation occupant population with a height of 1.750 m, BMI of 25.6 kg/m², and target age of 45 years [22]. The THUMS AM50 model represents an American 50th percentile male occupant based on one subject and was used as the reference model to morph to mid-size male anthropometry.

The models were selected due to their relevance for contemporary virtual safety assessment and their suitability for evaluating whole-body kinematics and region-specific injury metrics in frontal loading. Anatomical landmarks used for positioning workflows were defined in accordance with Euro NCAP CP 550 qualification procedures for human body models [1][3] and can be retrieved from Appendix A.

These landmark definitions ensured consistency with regulatory qualification requirements and enabled reproducible identification of corresponding anatomical locations across the VIVA+ 50M, HBM-Connect 50M, and reference THUMS models. Target coordinates for anatomical landmarks defining occupant posture were derived from the morphed THUMS 50M that had been previously positioned in the Toyota RAV4 driver seating position by researchers at the University of Michigan Transportation Research Institute (UMTRI) [29]. The THUMS model was morphed to mid-size male anthropometry and positioned using posture prediction methodologies developed at UMTRI. The reference midsize male geometry was generated using the UMTRI human skeleton and body surface models, which were developed from hundreds of computed tomography (CT) scans and body surface scans through principal component and regression analyses. Detailed descriptions of the geometry model are available in previous publications [28-33]. This UMTRI predicted midsize male geometry was used as the reference for morphing the THUMS v4.1 midsize male model. The same geometry also served as the basis for developing the HBM-Connect 50M model and, in part, the VIVA+ 50M model. Consequently, these three HBMs share similar skeletal structures and body shape geometries. The THUMS model was then positioned and settled within the RAV4 driving compartment model following the procedure described in [35]. A statistical seating posture model derived from volunteer seating posture data was used to predict the head and hip locations of a midsize male based on vehicle packaging parameters. The landmark coordinates were extracted from the reference posture and used as positioning targets for both VIVA+ 50M and HBM-Connect 50M. Importantly, the pelvic landmarks (ASIS-L/ASIS-R/pubic symphysis) provided the reference pelvic orientation used consistently across workflows, such that any differences in final pelvic angle arose from workflow sequence rather than from different intended target postures. The pelvic angle was defined as the angle between the plane formed by the left and right anterior superior iliac spines (ASIS) and the anterior-superior pubic symphysis, and the global vertical axis (Fig. 3).

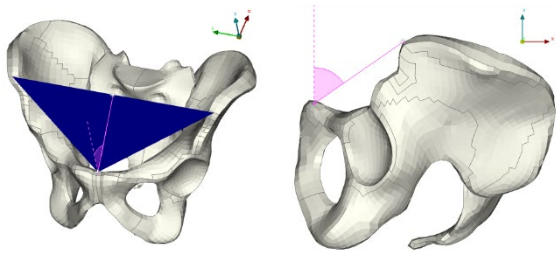

Fig. 3. Pelvic angle definition: plane formed by ASIS left and right and global vertical axis (THUMS pelvis).

The use of a positioned THUMS model as the source of target landmarks provided several methodological advantages. It ensured anatomical consistency and biomechanical plausibility of the target posture. Furthermore, it provided a unified reference posture enabling direct comparison between VIVA+ 50M and HBM-Connect 50M positioning outcomes. Finally, it established a baseline posture derived from validated posture prediction methodologies applied in automotive safety research.

Positioning Methodology

Two distinct positioning workflows were implemented to systematically investigate the influence of the positioning sequence on the pelvic angle and the resulting crash results. The workflows were each divided into two steps. After each step, the positioned HBMs, positioned in the RAV4 model, were simulated at two different speeds in a frontal load case. The workflows differed primarily in the order of positioning of the head, extremities and upper body, as well as in the adjustment methods of the pelvic alignment. At the start of all positioning, the HBMs were set to the correct H-point. The first positioning procedure initially involved positioning the head and extremities (“Upper-First”), followed by adjustment of the pelvis position (“Pelvis Correction”) in the second step. In the second positioning method, the pelvis and extremities were positioned first (“Pelvis-First”), followed by the head and upper body in the second step (“Thorax-Head Refinement”) (Fig 4). In the “Upper-First” (UF) positioning step, only the head (infraorbital) and extremities (HM_L/R, US_L/R, FE_L/R, IM_L/R) were positioned with beams (Appendix B). The pelvis, lumbar spine and thoracic spine were constrained in space. Rotation of the wrist and ankle was avoided. Based on the final position of the UF positioning step, the HBM positioning was completed in a second step using the “Pelvis Correction” (PC) positioning step. Here, the extremities (except femora), thoracic spine, cervical spine and skull were constrained in space, with the pelvis being rotated using beams to align with the target coordinates of the ASIS and pubic symphysis landmarks. In the “Pelvis- First” (PF) positioning step, the HBM was rotated around the H-point to achieve ASIS and pubic symphysis target coordinates, followed by the positioning of the extremities (HM_L/R, US_L/R, FE_L/R, IM_L/R), while the pelvis, spine and skull were constrained in space. Again, rotation of the wrist and ankle was avoided. Based on the final position of step PF, the head (head COG) and acromion were positioned, with only the X and Z coordinates being considered as positioning targets. During this positioning step “Thorax-Head Refinement” (TH), the lower extremities, hands, pelvis and lumbar spine were constrained in space. Visualisation of all positioning setups can be found in Appendix B.

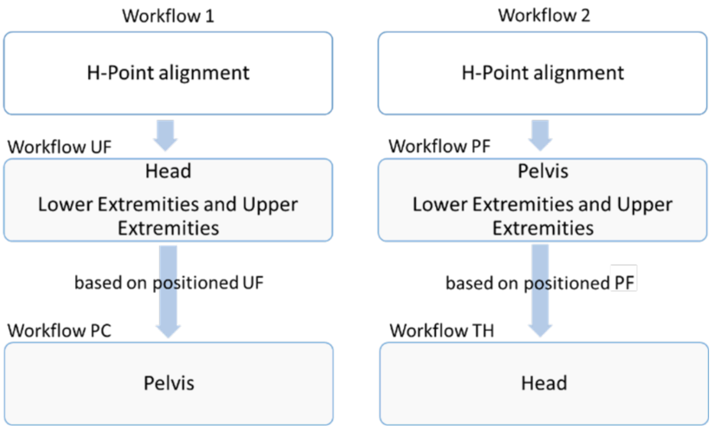

Fig. 4. Positioning workflows applied to VIVA+ 50M and HBM-Connect 50M.

The positioning was performed using simulation-based positioning with LS-DYNA R12.2 MPP single precision, where landmark targets were reached by either transforming the HBM or applying the marionette method (pre-simulation with pulling cables) and constraints while allowing the model to settle under contact and internal joint behaviour.

All three HBMs, in their various positions, were simulated in the Toyota RAV4 vehicle model in a frontal collision at two different speeds (32 and 61 km/h) [17]. All simulations used the same three-point seatbelt system, including a pretensioner triggered at 14 ms with a pretension force of 2.5 kN and a retractor with two active sensors. The time-based sensor was activated at 15 ms, after which the pullout-based sensor monitored belt pullout. The retractor locked when a maximum pullout of 2 mm was reached. The belt load limiter was defined by a force level of 3.75 kN at 0 mm belt pullout and 2.00 kN at 500 mm belt pullout. Belt material behaviour, retractor properties, pretensioner activation, and load-limiter settings were identical for all HBMs and positioning workflows. The results from VIVA+ and HBM-Connect were compared with their respective own results, with each other, and with the results from the THUMS midsize male. Just like the positioning simulations, the in-crash simulations were carried out with LS-Dyna R12.2. The results were analysed with the Dynasaur library. The overall rib fracture risk was evaluated using two strain-based rib fracture risk functions according to [36-37] for an age of 50 years, as [37] is a model-specific risk curve for the THUMS v4.1.

III. RESULTS

Human Body Model Positioning

The positioning procedures aimed to reproduce the target coordinates derived from defined landmarks of the positioned THUMS midsize male model. To evaluate the positioning accuracy, the resulting coordinates of selected anatomical landmarks were compared with the target coordinates from the THUMS reference model. The deviation between achieved and target coordinates was calculated for each workflow and each HBM compared to THUMS reference (Appendix D). Altogether, both models were able to reproduce the target posture with small deviations. However, differences were observed between the positioning workflows and between the two HBMs in terms of the remaining deviations from the target coordinates.

Overall, workflow 1 (consisting of UF and PC) resulted in smaller overall deviations from the target coordinates than workflow 2 (consisting of PF and TH). The final positioning achieved with workflow 1 showed the lowest average landmark deviations across the evaluated anatomical points. Looking specifically at pelvic positioning, smaller deviations were observed for pelvic landmarks in workflow 1, whereas head-related landmarks showed smaller deviations in workflow 2.

Furthermore, differences in positioning accuracy were observed between the VIVA+ 50M and HBM-Connect 50M models. For VIVA+, a clear workflow-dependent pattern emerged. The first workflow resulted in lower overall deviations, with mean absolute total coordinate deviations of 1.1 mm for both, UF and PC, whereas the second workflow produced larger deviations of 1.7 mm for PF and 1.9 mm for TH. Thus, in VIVA+, the workflow based on upper-body-first positioning reproduced the target coordinates more accurately than the workflow starting from the extremities. In HBM-Connect 50M, this pattern was less pronounced. The lowest total mean deviation was obtained for UF at 1.0 mm, while PC showed the largest deviation at 1.6 mm. PF and TH both resulted in intermediate values of 1.4 mm. Compared with VIVA+, HBM-Connect therefore showed a less consistent separation between the two workflows, although deviations in the z-direction tended to be larger in the second workflow, particularly for TH. Despite the overall good positioning accuracy observed for both HBMs, it could be seen, that VIVA+ 50M generally tended to show smaller deviations for pelvic and thorax related landmarks, while the HBM-Connect 50M model resulted in smaller deviations for selected lower extremity landmarks. Pelvic angle varied substantially between the models and across positioning workflows.

TABLE I
PELVIC ANGLES ACROSS POSITIONING STEPS

Model	Default	UF	PC	PF	TH	THUMS reference
VIVA+ 50M	54.65°	59.59°	58.54°	55.70°	55.70°	55.23°
HBM-Connect 50M	39.83°	47.71°	53.97°	57.79°	57.79°	55.23°

The largest workflow-related variation was observed for HBM-Connect 50M, for which the pelvic angle ranged from 39.83° in the default configuration to 57.79° after TH. In contrast, VIVA+ 50M showed a narrower range, from 54.65° in the default position to 59.59° after UF. Relative to the THUMS reference pelvic angle of 55.23°, the default VIVA+ posture was already close to the target, whereas HBM-Connect started from a markedly lower pelvic angle and showed larger workflow-dependent changes. Overall, the applied workflows altered pelvis orientation in both HBMs, but the effect was more pronounced in HBM-Connect than in VIVA+. Further supporting illustrations of the positioning process and the coordinates achieved can be found in Appendices C and D.

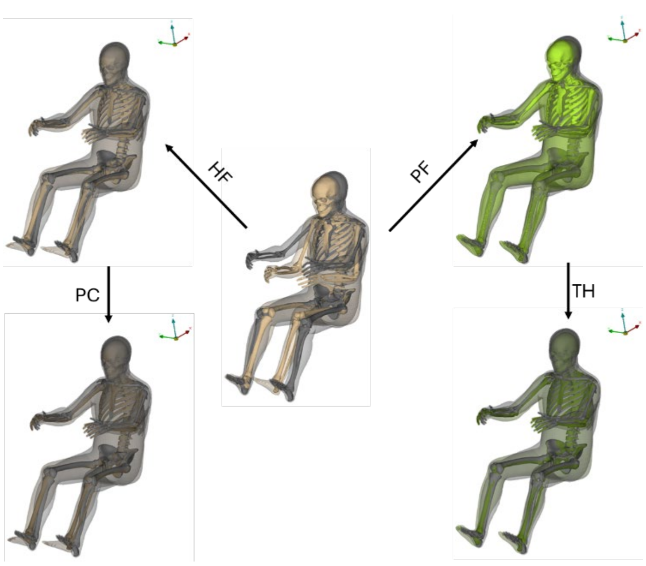

Fig. 5. THUMS midsize male positioned (gray) and VIVA+ 50M after each positioning step.

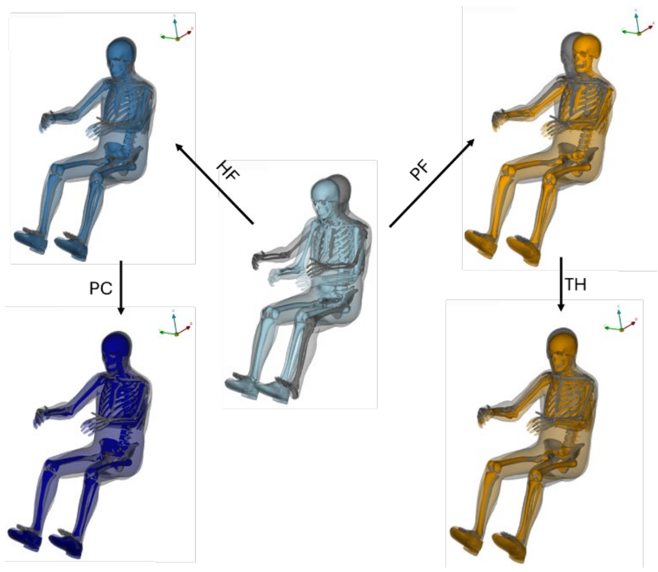

Fig. 6. THUMS midsize male positioned (gray) and HBM-Connect 50M after each positioning step.

Frontal Crash Simulations

For the belt forces, the shoulder belt response was broadly consistent across models and positioning steps, with only minor variation at both impact severities. At 32 km/h, both HBMs remained close to the THUMS level of 3.75 kN, with values clustered between 3.92 kN and 4.00 kN. A similarly small spread was observed at 61 km/h, where all model responses remained close to the THUMS value of 3.76 kN and varied only between 4.02 kN and 4.12 kN. Overall, shoulder belt force showed little sensitivity to positioning workflow and only limited differences between HBMs. In contrast, larger differences were observed for the lap belt force, particularly at 61 km/h. At 32 km/h, both HBMs remained close to the THUMS value of 2.59 kN, although HBM-Connect tended to be slightly lower and VIVA+ spanned both slightly lower and slightly higher values depending on workflow. At 61 km/h, however, both HBMs exceeded the THUMS response of 3.87 kN in all workflows. The highest lap belt force was observed in VIVA+ in workflow UF at 5.69 kN, whereas the maximum in HBM-Connect reached 4.86 kN in PC. Thus, compared with the shoulder belt force, the lap belt force showed clearer model- and workflow-dependent differences, with the strongest increase occurring in VIVA+ at the higher impact speed.

For the lower extremities, femur forces showed relatively limited workflow sensitivity compared with the tibia forces, while model-related differences were already evident at 32 km/h. The most notable deviation occurred for the right femur in HBM-Connect, where forces reached up to 1.60 kN, compared with 0.65 kN in THUMS. In contrast, VIVA+ remained much closer to the THUMS level on the right side, while both HBMs produced slightly higher forces on the left. At 61 km/h, femur loading increased in all models, but the overall pattern remained similar. VIVA+ stayed below THUMS on both sides, whereas HBM-Connect approached the THUMS level more closely on the left and reached its highest value in TH at 5.96 kN, slightly exceeding the THUMS response of 5.39 kN. Overall, femur forces were influenced more by model choice than by positioning workflow.

The tibia forces showed clearer differences between models and stronger workflow dependence. At 32 km/h, both HBMs exceeded the THUMS values for both upper and lower tibia forces in all positioning steps, with the largest deviations observed on the left side. This was particularly pronounced for the upper left tibia, where VIVA+ reached 1.73 kN and HBM-Connect 1.66 kN, compared with 0.75 kN in THUMS. The clearest workflow effect was observed for the lower left tibia. In VIVA+, this force increased from 3.12 kN in UF to 4.05 kN in TH, and in HBM-Connect from 3.09 kN in PC to 3.59 kN in TH, indicating that TH consistently produced the highest distal tibia loading at the higher impact speed. On the right side, the upper tibia forces in both HBMs also remained above the THUMS level.

In summary, the lower extremity response was characterised by comparatively modest workflow effects for femur loading, but distinctly larger model- and workflow-dependent differences for tibia loading, especially on the left side and at 61 km/h.

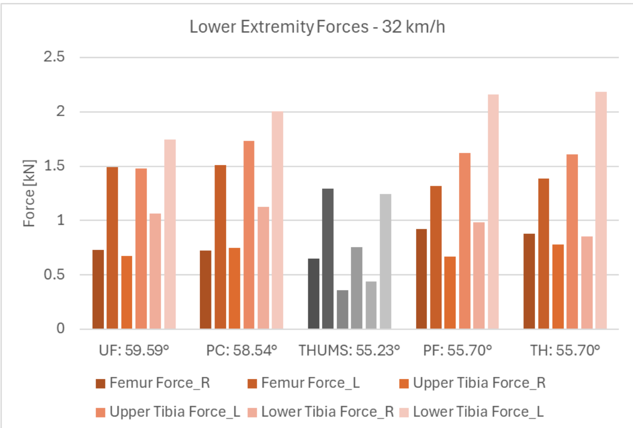

Fig. 7. Lower Extremity Forces of VIVA+ 50M for each pelvic angle at 32km/h compared to THUMS reference model.

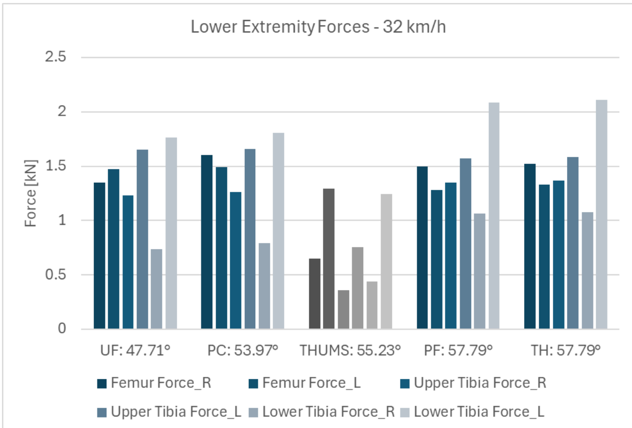

Fig. 8. Lower Extremity Forces of HBM-Connect 50M for each pelvic angle at 32km/h compared to THUMS reference model.

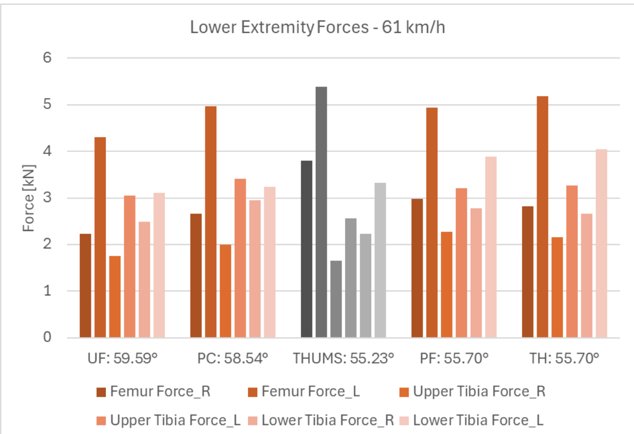

Fig. 9. Lower Extremity Forces of VIVA+ 50M for each pelvic angle at 61km/h compared to THUMS reference

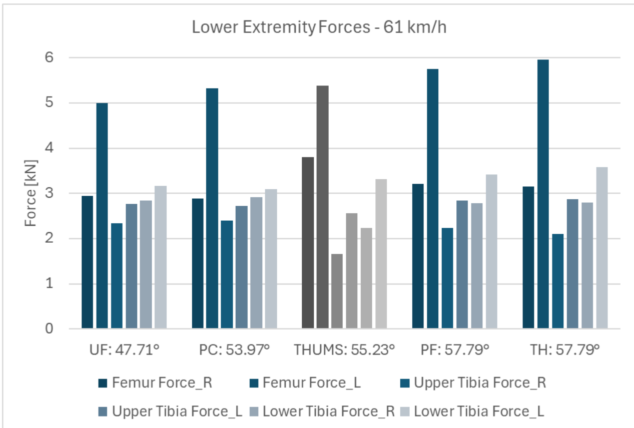

Fig. 10. Lower Extremity Forces of HBM-Connect 50M for each pelvic angle at 61km/h compared to THUMS

model. reference model.

For thoracic response, the THUMS maximum chest deflection was 30.9 mm at 32 km/h and 36.7 mm at 61 km/h. In VIVA+, chest deflection ranged from 42.7 mm in step TH to 51.08 mm in step PF at low speed and from 49.9 mm in step TH to 57.9 mm in step PF at high speed. In HBM-Connect, the corresponding values ranged from 54.8 mm in step UF to 57.7 mm in step PC at 32 km/h and from 46.6 mm in step PF to 60.6 mm in positioning step UF at 61 km/h. The rib maximum principal strain results showed a maximum THUMS value of 0.011 at low speed, occurring at R3 and R5, and 0.019 at high speed at L1. In VIVA+, the maximum rib strain at 32 km/h was 0.05 at L1 in step UF, and at 61 km/h it was 0.055 L1 in step PC. In HBM-Connect, the maximum rib strain was 0.099 at L1 in positioning step TH at low speed and 0.103 at R1 in positioning steps UF and PC at high speed.

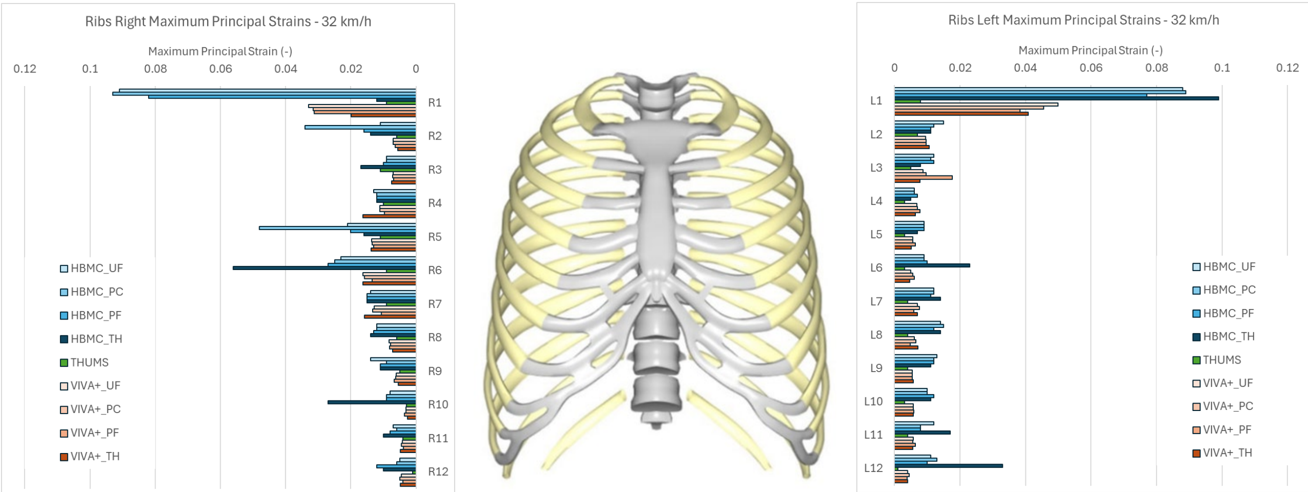

Fig. 11. Maximum principal strains of individual ribs per HBM, workflow and THUMS reference at 32 km/h based on [36].

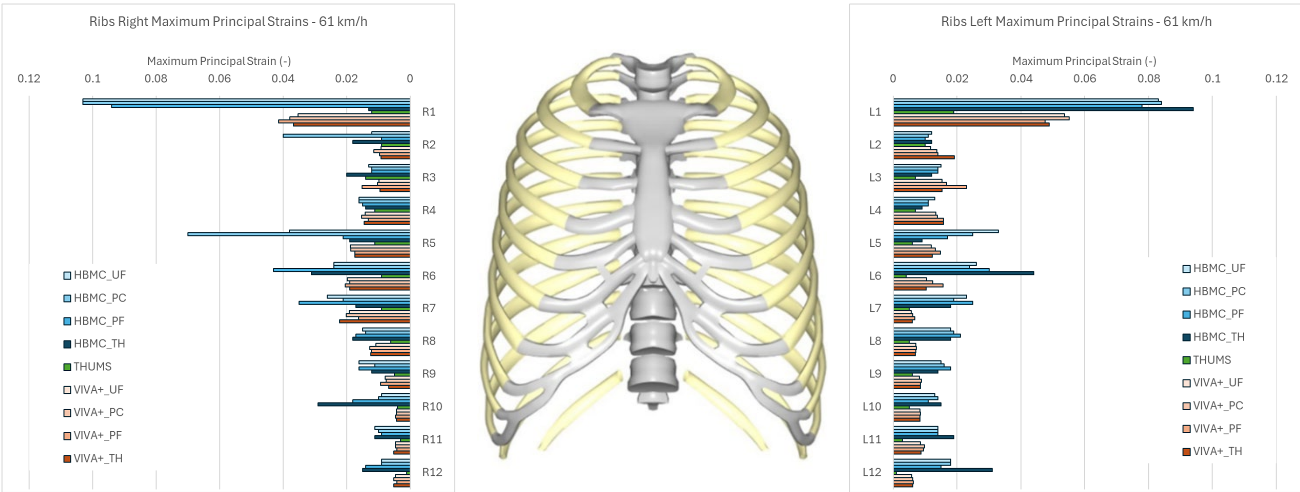

Fig. 12. Maximum principal strains of individual ribs per HBM, workflow and THUMS reference at 61 km/h based on [36].

Based on [36], for THUMS, the risk to fracture three or more ribs (NFR=3+) was zero at both velocities. VIVA+ ranged from 5% in step UF to 13% in PF at low speed and from 43% in positioning step UF to 70% in PF at high speed. HBM-Connect ranged from 53% in step UF to 99% in PC at 32 km/h and from 98% in step TH to 100% in PC at 61 km/h. Based on [37], for THUMS, the risk to fracture three or more ribs (NFR=3+) was 9% at low speed and 30% at high speed. VIVA+ ranged from 84% in UF and TH to 87% in step PF at low speed and from 99% in UF to 100% in positioning step PF at high speed. HBM-Connect ranged from 94% in UF to 100% in step PC and TH at 32 km/h and showed 100% NFR3+ risk in all positioning steps at 61 km/h.

For the head-related metrics, THUMS yielded a HIC_{15} (Head Injury Criterion) value of 66 at 32 km/h and 419 at 61 km/h. In the low-speed condition, VIVA+ ranged from 47 in step PF to 63 in PC, whereas HBM-Connect ranged from 51 in UF to 62 in TH. At 61 km/h, the VIVA+ values ranged from 202 in UF to 240 in TH. HBM-Connect ranged from 313 in step TH to 435 in PF. The HIC_{15}-based AIS3+ injury risk was very low throughout all positioning steps for all HBMs. The THUMS was below 3% at 61 km/h. The risk for VIVA+ was below 1% in UF and TH at high speed. HBM-Connect ranged from 1% in step TH to 3% in PF at 61 km/h. HIC_{15}-based AIS3+ injury risk was zero for all models at low speeds. For DAMAGE-based AIS2 injury risk, the THUMS reference values were close to 0%. VIVA+ showed 3% DAMAGE-based AIS2 injury risk in UF at low speed and 80% in PC at high speed. As THUMS, HBM-Connect showed 0% injury risk at 32 km/h, but ranged from 1% in UF to 35% in PF at 61 km/h.

IV. DISCUSSION

The present study assessed whether different positioning workflows affected positioning accuracy, pelvic angle and subsequent crash injury response of the VIVA+ 50M and HBM-Connect 50M models when aligned to a positioned THUMS midsize male reference model. In terms of landmark-based positioning accuracy, both HBMs reproduced the target posture well. Positioning flows UF and PC (workflow 1) represented a two-stage sequential process in which the head and extremities were positioned before the pelvic landmarks where aligned. Steps PF and TH (workflow 2) represented an alternative two-stage process in which the pelvic and extremity positioning preceded that of the upper body. Across all positioning steps, the mean absolute total coordinate deviation was 1.45 mm for VIVA+ 50M and 1.42 mm for HBM-Connect 50M, indicating that both models could be positioned close to the prescribed THUMS target coordinates. Workflow 1 generally resulted in smaller overall deviations than workflow 2, although this difference was more pronounced for VIVA+ 50M than for HBM-Connect 50M. Furthermore, the distribution of these deviations across anatomical regions differed between workflows, with workflow 1 showing smaller pelvic deviations and workflow 2 showing smaller head-related deviations. This suggests that positioning accuracy cannot be judged solely on the basis of a single global error measure, as improvements in one region may occur at the expense of another. This becomes especially relevant when considering pelvic orientation. Despite the generally small landmark deviations, the pelvic angle differed notably between the two HBMs and across the workflows. In VIVA+ 50M, the default pelvic angle was already close to the THUMS reference and remained within a relatively narrow range after positioning steps. In contrast, HBM-Connect 50M started from a markedly lower default pelvic angle and showed a much larger workflow-dependent change before approaching the THUMS value. These findings indicate that close agreement in selected landmark coordinates does not necessarily correspond to equivalent segment orientation and that workflow choice can alter pelvic angle within the same HBM, even when external geometric matching remains good. The crash results indicate that these within-model workflow differences were not merely geometric, but biomechanically relevant. In both HBMs, workflow-dependent changes in pelvic angle coincided with changes in lap belt force and lower-extremity loading, particularly in the femur and tibia forces. This within-model pattern was clearer and more interpretable than many of the absolute differences between HBMs, because it suggests that workflow choice altered pelvis-belt interaction and subsequent load transfer through the lower body. The lap belt force is especially informative in this regard, as it provides a direct mechanical link between pelvis orientation and restraint engagement. The fact that changes in lap belt force were accompanied by changes in femur and tibia loading supports the interpretation that workflow-induced changes in pelvic posture influenced downstream loading paths. At the higher impact speed, workflow-dependent differences were also observed in thoracic and head-related criteria, indicating that these posture-related effects may propagate beyond the pelvis and lower extremities as crash severity increases.

The crash results further showed that the effect of positioning was not uniform and predictable across metrics or models. For the head-related criteria, workflow dependent differences were observed in both HBMs, particularly at 61 km/h. HBM-Connect 50M generally produced HIC15 and HIC15-based AIS3+ injury risk values closer to those of THUMS than VIVA+ 50M. The higher DAMAGE-based AIS2 injury risk values in the VIVA+ model can be attributed primarily to the significantly “soft” neck modelling in VIVA+. Nevertheless, both HBMs predicted substantially higher DAMAGE-based AIS2 injury risk values than THUMS at both impact severities. This indicates that the extent of agreement with the THUMS reference depended on the chosen injury metric. It also suggests that translationally dominated and strain- or rotation-related head injury measures did not respond in the same way to the workflow-induced posture changes and to the underlying model characteristics. THUMS therefore cannot be regarded as a simple numerical target across all head-related criteria. Rather, the comparison demonstrates that each model responds differently depending on the metric considered.

A similarly clear model dependency was found for the thoracic response. Both HBMs predicted larger chest deflections and higher local rib strains than THUMS, while THUMS yielded the lowest NFR3+ risks at both velocities for both rib risk curves. Based on the model characteristics, this behaviour is mechanically plausible.

The comparatively large rib cross-sections in THUMS make the chest stiffer than in VIVA+ 50M and HBM-Connect 50M, which is expected to reduce local rib deformation and the associated strain values. Furthermore, the modelling of the soft tissue and adipose tissue of the THUMS thorax suggests that the transfer of strain from the surrounding soft tissue to the ribs is less pronounced in THUMS than in the other two HBMs. For example, the soft tissue around the THUMS thorax at the level of the shoulder girdle across the sternum is three times as thick as in the HBM-Connect, and compared to the VIVA+, the material formulation is also different. Consequently, part of the soft tissue strain distribution appeared to be lost before it reached the rib structure [37–38]. Together, these factors provide a plausible explanation for the lower maximum principal strains in the THUMS ribs and, consequently, for the lower NFR3+ risks based on [38–39]. This finding underlines that strain-based thoracic criteria are particularly sensitive to differences in rib geometry, structural stiffness, and soft-tissue representation. That is why it is important to compare the results within the HBMs. In this regard, it was observed that HBM-Connect responded considerably more sensitively to varied positioning workflows in terms of rib strain than VIVA+.

The lower extremity and belt force results were consistent with the same overall interpretation. In both HBMs, femur and tibia forces as well as shoulder and lap belt forces varied across positioning steps, but the position of the THUMS reference within these ranges depended on the criterion, the body side, and the impact speed. This indicates that the influence of positioning cannot be reduced to a simple increase or decrease in loading. Instead, the workflows appear to have redistributed load transfer through the restraint system and the lower body. The lap belt force is especially relevant in this respect, because it provides a direct mechanical link between pelvic angle and occupant loading. The fact that changes in lap belt force coincided with changes in femur and tibia loading supports the view that workflow-induced differences in pelvic orientation contributed to altered pelvis-belt interaction and downstream load paths.

Summarised, the present results support pelvic angle as a useful descriptor of biomechanically relevant initial posture, because it changed within the same model across workflows and these changes were accompanied by differences in restraint force and lower-extremity loading. However, pelvic angle should not be interpreted as the sole explanatory factor. A further challenge in comparing the HBMs is that pelvic bone geometry also differs between models and may affect the final pelvis orientation and thus lap belt engagement. The geometry of the ASIS region and notch is likely to be especially relevant in this context, because it influences lap belt interaction with the pelvis. Accordingly, some of the observed differences in belt loading and subsequent injury response cannot be attributed to pelvic angle alone, but likely reflect the combined influence of posture and model specific local anatomy.

Furthermore, several limitations should be considered. First, the effect of the pelvic angle was not completely isolated from other changes in position caused by the workflows, even though these changes were only minor. Therefore, it is possible that the observed correlations are part of a coupled positioning effect and should not be viewed prematurely as evidence of a causal mechanism based on a single variable. Secondly, the analysis was limited to two HBMs, positioning workflows were not performed on THUMS, in frontal impact simulations at 32 and 61 km/h. Even so, the consistency of the observed trends across restraint forces, lower-extremity loads, thoracic deformation, and selected head criteria indicates that workflow-induced posture differences, particularly in the pelvis, are relevant for the interpretation of HBM-based crash simulations.

These findings are also relevant in the context of the Euro NCAP virtual testing roadmap. Euro NCAP currently uses HBM simulations for monitoring purposes and aims to incorporate HBM simulations into the assessment framework for 2029. At the same time, the current protocol emphasises the need for transparent and standardised procedures. Against this background, the present results suggest that predefined positioning workflows and their influence on biomechanically relevant posture descriptors, particularly pelvic angle, should be borne in mind when developing and interpreting HBM-based assessments for the planned 2029 implementation [1–2].

V. CONCLUSION

Both VIVA+ 50M and HBM-Connect 50M were positioned with small landmark deviations relative to the THUMS-based target posture, and workflow 1 (UF/PC) generally achieved slightly better overall coordinate agreement than workflow 2 (PF/TH). However, the positioning results also showed that good external landmark matching did not necessarily result in equivalent internal posture. In particular, the pelvic angle differed

considerably between the two HBMs, with VIVA+ 50M remaining close to the THUMS reference and HBM-Connect 50M showing a much larger shift from its default posture. These posture differences were reflected in the in-crash simulations. Injury metrics, thoracic response, lower-extremity forces, and belt forces all varied with workflow, showing that the positioning method influenced the subsequent occupant response at both velocities applied. The associated changes in lap belt, femur, and tibia loading indicate that pelvic orientation was an important part of the kinematic chain linking initial posture to restraint interaction and injury outcome.
Furthermore, the comparison with THUMS has shown that workflow effects must be interpreted in the context of model-specific characteristics. HBM-Connect 50M approached THUMS more closely for some HIC-based head metrics at high speed, whereas both HBMs predicted substantially higher DAMAGE-based AIS2 injury risk values than THUMS. For thoracic response, both HBMs showed greater chest deflection and rib strain, while THUMS consistently produced lower NFR3+ risks. These differences are consistent with the stiffer thoracic behaviour of THUMS, which is likely related to its larger rib cross-sections and to differences in soft-tissue-to-rib strain transfer.
Overall, the findings show that HBM positioning should not be evaluated solely on the basis of external landmark accuracy. Biomechanically relevant posture descriptors, in particular pelvic angle, should also be considered, as they may substantially affect restraint system engagement and injury prediction. In addition, cross-model comparisons should be interpreted with caution, since differences in anatomy, structural stiffness, and material behaviour can strongly influence predicted injury metrics even when the prescribed target posture is reproduced closely. This is of great significance for the planned integration of HBM simulations into Euro NCAP assessments starting in 2029, in which positioning procedures and their effects on pelvic orientation should be explicitly taken into account.

VI. ACKNOWLEDGEMENTS

The authors would like to thank Humanetics for providing a licence for the HBM-Connect model. They also acknowledge the use of the high-performance computing resources provided by the IT Services (ZID) at Graz University of Technology.

VII. REFERENCES

[1] Euro NCAP. (2025) *Qualification Procedure for Human Body Models*. Technical Bulletin CP 550, v1.1.

[2] Euro NCAP. (2025) *Human Body Model Simulations in Frontal Impacts*. Technical Bulletin CP 551, v1.1.

[3] Klein, C., González-García, M., *et al*. (2021) A Method for Reproducible Landmark-based Positioning of Multibody and Finite Element Human Models. *Proceedings of the IRCOBI Conference*, 2021, online.

[4] Li, X., Yuan, Q., *et al.* (2023) Personalization of human body models and beyond via image registration. Frontiers in Bioengineering and Biotechnology, **11**: p.1169365.

[5] VIRTUAL-OSCCAR workshop. (2020) *Virtual Testing Methods and Tools for Advanced Crash Protection*.

[6] Piqueras, A., Iraeus, J., Pipkorn, B., López-Valdés, F. J. (2023) Assessment of the sensitivity of thoracic injury criteria to subject-specific characteristics using human body models. Frontiers in Bioengineering and Biotechnology, **11**: p.1106554.

[7] Brynskog, E., Iraeus, J., Pipkorn, B., Davidsson, J. (2024) Simulating Pelvis Kinematics from Belt and Seat Loading in Frontal Car Crash Scenarios: Important Boundary Conditions that Influence the Outcome. Annals of Biomedical Engineering, **53**(2): pp.441–470.

[8] Brynskog, E., Östh, J., Larsson, K.-J., Iraeus, J. (2025) Effect of occupant and restraint variability in reclined positions on submarining probability in frontal car crash scenarios. Frontiers in Bioengineering and Biotechnology, **13**: p.1570572.

[9] Grébonval, C., Trosseille, X., Petit, P., Wang, X., Beillas, P. (2021) Effects of seat pan and pelvis angles on the occupant response in a reclined position during a frontal crash. PLOS ONE, **16**(9): p.e0257292.

[10] Leledakis, A. (2024) *Heterogeneity in car occupant safety : using numerical simulations to address real world safety*, Chalmers University of Technology.

[11] Erlinger, N., Kofler, D., Heider, E., Klug, C. (2022) Effects of Boundary Conditions and Posture on Simulations with Human Body Models of Braking Events. *Proceedings of the IRCOBI Conference*, 2022, Porto, Portugal.

[12] Poulard, D., Subit, D., Nie, B., Donlon, J.-P., Kent, R. W. (2015) The Contribution of Pre-impact Posture on Restrained Occupant Finite Element Model Response in Frontal Impact. Traffic Injury Prevention, 16(2): pp. S87–S95

[13] Poulard, D., Subit, D., Donlon, J.-P., Lessley, D. J., Kim, T., Park, G., Kent, R. W. (2014) The Contribution of Pre-impact Spine Posture on Human Body Model Response in Whole-body Side Impact. Stapp Car Crash Journal, **58**: pp. 385–422.

[14] Larsson, E., Iraeus, J., Davidsson, J. (2023) Investigating sources for variability in volunteer kinematics in a braking maneuver, a sensitivity analysis with an active human body model. Frontiers in Bioengineering and Biotechnology, **11**: p. 1203959.

[15] Bose, D., Crandall, J. R., Untaroiu, C. D., Maslen, E. H. (2010) Influence of pre-collision occupant parameters on injury outcome in a frontal collision. Accident Analysis and Prevention, **42**(4): pp. 1398–1407.

[16] Gaewsky, J. P., Weaver, A. A., Koya, B., Stitzel, J. D. (2015) Driver Injury Risk Variability in Finite Element Reconstructions of Crash Injury Research and Engineering Network (CIREN) Frontal Motor Vehicle Crashes. Traffic Injury Prevention, **16**(2): pp. S124–S131.

[17] Gierczycka, D., Cronin, D. S. (2017) Occupant thorax response variations due to arm position and restraint systems in side impact crash scenarios. Accident Analysis and Prevention, **106**: pp.173–180.

[18] Bohman, K., Fågelberg, E., Jakobsson, L. (2023) Investigating Slouching in Frontal Impacts Using an HBM in the Rear Seat. *Proceedings of the Enhanced Safety of Vehicles (ESV) Conference*, 2023, Yokohama, Japan.

[19] Svenning, E., Mroz, K., Johansen, T., Lübbe, N., Iraeus, J. (2021) Comparing the Frontal Impact Responses of the VIVA+ Average Female and SAFER Average Male Human Body Models in a Generic Seat. *13th European LS-DYNA Conference*, 2021, Ulm, Germany.

[20] Reed, M. P., Manary, M. A., Flannagan, C. A. C., Schneider, L. W. (2002) A Statistical Method for Predicting Automobile Driving Posture. Human factors, **44**(4): pp.557–568.

[21] John, J., Klug, C., Kranjec, M., Svenning, E., Iraues, J. (2022) Hello, World! VIVA+: A Human Body Model Lineup to Evaluate Sex-Differences. Frontiers in Bioengineering and Biotechnology, **10**: p.918904.

[22] Humanetics. “HBM CONNECT® 50TH MALE”, https://www.humaneticsgroup.com/products/virtual-models/hbm-connect/hbmc-50th-male#paragraph-spacer-21474. [cited 2026-06-03]

[23] Boyle, K., Hu, J., Reed, M. P., Rupp, J. (2024) Development of Parametric Finite Element Vehicle and Restraint Models for Occupant Protection Research. *Proceedings of the IRCOBI Conference*, 2024, Stockholm, Sweden.

[24] Hu, J., Lin, C., Reed, M.P., Boyle, K. (2025) *NHTSA HBM Virtual Testing Framework*.

[25] Iraeus, J., Lindquist, M. (2015) Pulse shape analysis and data reduction of real-life frontal crashes with modern passenger cars. International Journal of Crashworthiness, **20**(6): pp. 535–546.

[26] Schneider, L. W., Robbins, D. H., Pflug, M. A., Snyder, R. G. (1983) Development of anthropometrically based design specifications for an advanced adult anthropomorphic dummy family, **1**(UMTRI-83-53-1), University of Michigan Transportation Research Institute, Ann Arbor, MI.

[27] United States Department of Health and Human Services, National Center for Health Statistics. (1992) National Health and Nutrition Examination Survey I, 1971–1975: Anthropometry, Goniometry, Skeletal Age, Bone Density, and Cortical Thickness. Inter-university Consortium for Political and Social Research. https://doi.org/10.3886/ICPSR08058.v2

[28] Brynskog, E., Iraeus, J., Reed, M.P., Davidsson, J. (2021) Predicting pelvis geometry using a morphometric model with overall anthropometric variables. Journal of Biomechanics, **126**: p. 110633.

[29] Hu, J., Dhawan, M., Fan, X., Reed, M.P. (2022) Toward Improved Safety Equity: An Efficient, Parametric, and Posable Finite Element Human Model Representing a Diverse Population. *Proceedings of the IRCOBI Conference,* 2022, Porto, Portugal.

[30] Klein, K.F., Hu, J., Reed, M.P., Hoff, C.N., Rupp, J.D. (2015) Development and Validation of Statistical Models of Femur Geometry for Use with Parametric Finite Element Models. Annals of Biomedical Engineering, **43**(10): pp 2503-2514.

[31] Park, B.K., Jones, M., Ebert, S., Reed, M.P. (2021) A parametric modeling of adult body shape in a supported seated posture including effects of age. Ergonomics, **65**(6): pp 795-803.

[32] Tang, L., Hu, Z., Lin, Y., Hu, J. (2022) A Statistical Lumbar Spine Geometry Model Accounting for Variations by Age, Sex, Stature, and Body Mass Index. Journal of Biomechanics. **130**: p. 110821.

[33] Wang, Y., Cao, L., Bai, Z., Reed, M.P., Rupp, J.D., Hoff, C.N., Hu, J. (2016) A Parametric Ribcage Geometry Model Accounting for Variations among the Adult Population. Journal of Biomechanics, **49**(13): 2791-2798.

[34] Wei, A., Wang, J., Liu, J., Jones, M., Hu, J. (2022) A parametric head geometry model accounting for variation among adolescent and young adult populations. Computer Methods and Programs in Biomedicine, 220: p. 106805. DOI: 10.1016/j.cmpb.2022.106805

[35] Hu, J., et al. (2019) Frontal crash simulations using parametric human models representing a diverse population. Traffic Injury Prevention 20(sup1): s97-s105.

[36] Larsson, K.J., Blennow, A., Iraeus, J., Pipkorn, B., Lübbe, N. (2021) Rib Cortical Bone Fracture Risk as a Function 453 of Age and Rib Strain: Updated Injury Prediction Using Finite Element Human Body Models. Frontiers in 454 Bioengineering and Biotechnology, 9: p.677768.

[37] Forman, J., Kulkarni, S., et al. (2022) A Method for Thoracic Injury Risk Function Development for Human Body Models. *Proceedings of the IRCOBI Conference*, 2022. Porto, Portugal.

[38] Kannan, V., Ressi, F., Klug, C. (2025) Strain-based risk fracture evaluation with freely available HBMs – A comparison against reference PMHS tests. *Proceedings of the IRCOBI Conference*, 2025, Vilnius, Lithuania.

[39] Holcombe, S., Huang, Y. (2023) Cross-sectional properties of rib geometry from an adult population. Frontiers in Bioengineering and Biotechnology, 11: p. 1158242.

VIII. APPENDIX

A) Target Landmarks and Definition

TABLE A-I
POSITIONING LANDMARKS

Landmark	Definition
H-Point	Centre of the right and left acetabulum centres
ASIS-R	Node on right anterior superior iliac spine
ASIS-L	Node on left anterior superior iliac spine
Pubic Symphysis	Node on most cranial point of pubic symphysis
HM_R	Midpoint of the most caudal-lateral and caudal-medial point on lateral epicondyle of the humerus, right
HM_L	Midpoint of the most caudal-lateral and caudal-medial point on lateral epicondyle of the humerus, left
US_R	Tip of ulnar styloid, right
US_L	Tip of ulnar styloid, left
Acromion_R	Most distal node on right acromion
Acromion_L	Most distal node on left acromion
FE_R	Midpoint of lateral and medial femoral epicondyle, right
FE_L	Midpoint of lateral and medial femoral epicondyle, left
IM_R	Inter-malleolar point, right
IM_L	Inter-malleolar point, left
Head COG	Centre of gravity of the head
Infraorbitale	Centre of infraorbital ridge

B) Positioning Set-Ups

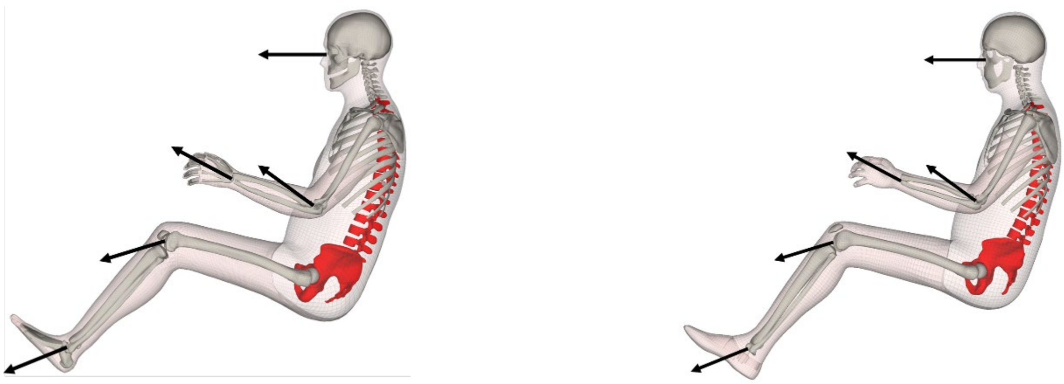

Fig. B-1. Set-Up for workflow “Upper-First” (UF) for VIVA+ 50M (left) and HBM-Connect 50M (right). Bones which were constrained during positioning workflow are coloured in red.

Fig. B-2. Set-Up for workflow “Pelvis Correction” (PC) for VIVA+ 50M (left) and HBM-Connect 50M (right). Bones which were constrained during positioning workflow are coloured in red.

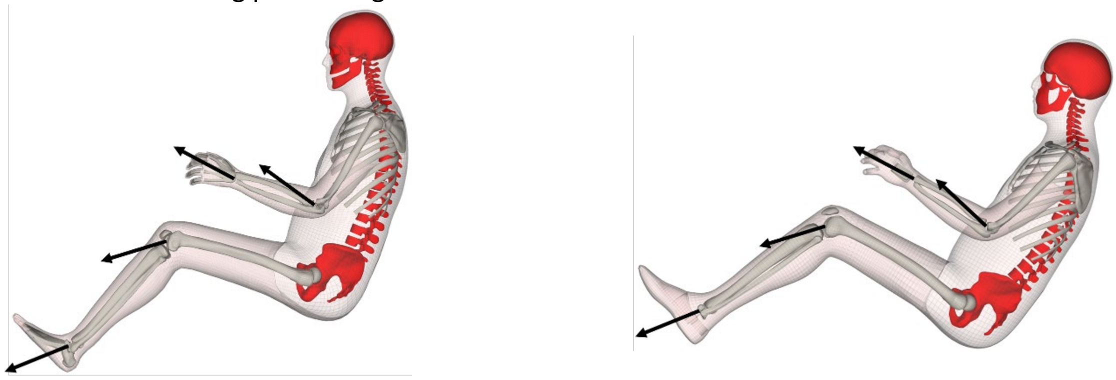

Fig. B-3. Set-Up for workflow “Pelvis-First” (PF) for VIVA+ 50M (left) and HBM-Connect 50M (right). Human Body Models already rotated around H-Point for pelvis landmark alignment. Bones which were constrained during positioning workflow are coloured in red.

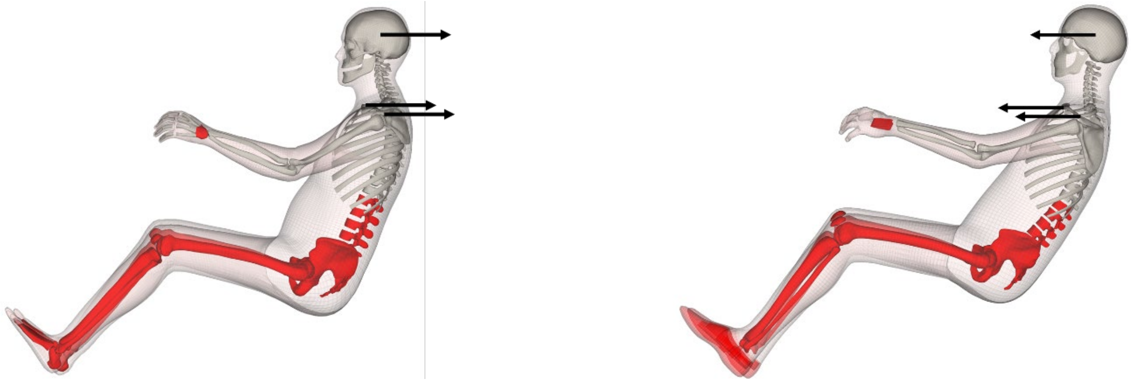

Fig. B-4. Set-Up for workflow “Thorax-Head Refinement” (TH) for VIVA+ 50M (left) and HBM-Connect 50M (right). Human Body Models already rotated around H-Point for pelvis landmark alignment. Bones which were constrained during positioning workflow are coloured in red.

C) HBM Positioning Results

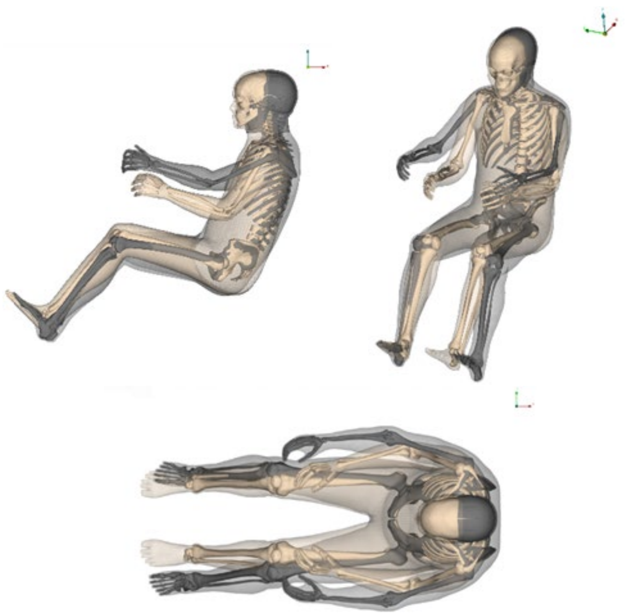

Fig. C-1. THUMS midsize male positioned (gray) and VIVA+ 50M v.2.0.1 in default position (light beige).

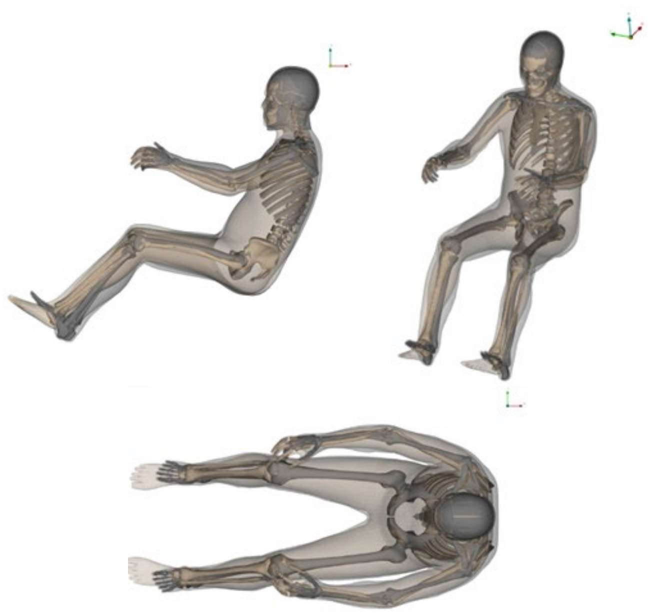

Fig. C-2. THUMS midsize male positioned (gray) and VIVA+ 50M v.2.0.1 after positioning workflow UF (middle beige) and PC (dark beige).

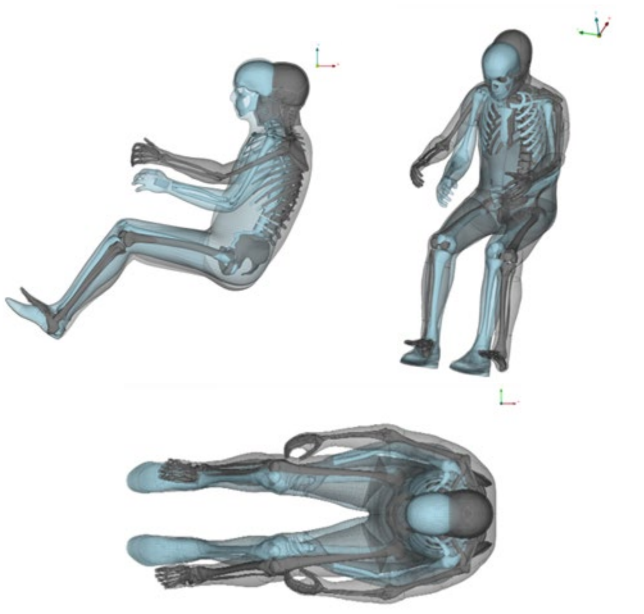

Fig. C-3. THUMS midsize male positioned (gray) and HBM-Connect 50M v2.5 in default position (lightblue).

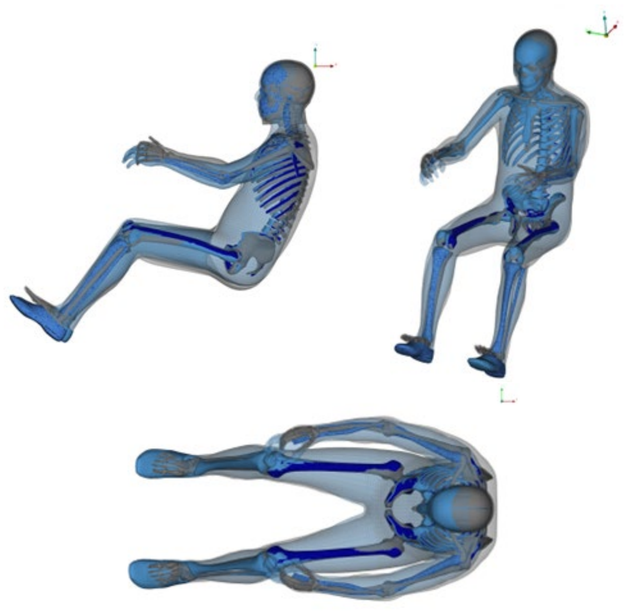

Fig. C-4. THUMS midsize male positioned (gray) and HBM-Connect 50M v2.5 after positioning workflow UF (middle blue) and PC (dark blue).

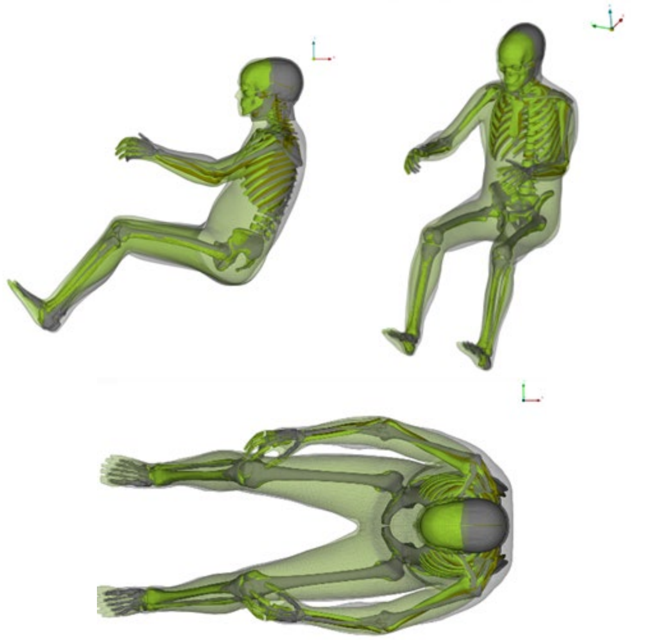

Fig. C-5. THUMS midsize male positioned (gray) and VIVA+ 50M v.2.0.1 after positioning workflow PF (middle green) and TH (dark green).

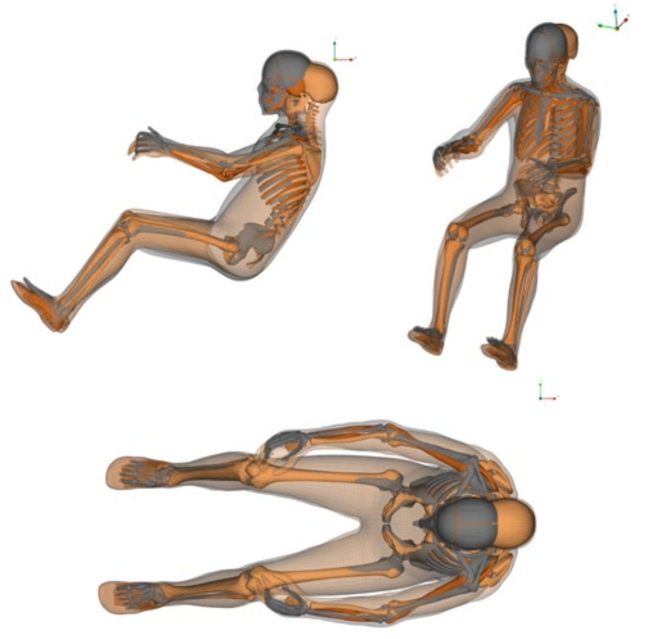

Fig. C-6. THUMS midsize male positioned (gray) and HBM-Connect 50M v2.5 after positioning workflow PF (middle orange) and TH (dark orange).

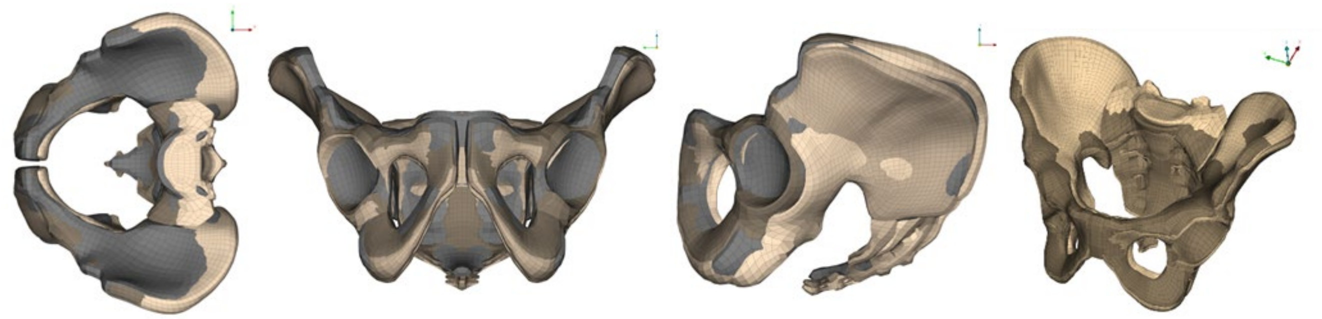

Fig. C-7. Pelvis orientation: THUMS midsize male positioned (gray), VIVA+ 50M v2.0.1 pelvis in default position (light beige), after positioning workflow UF (middle beige), after positioning workflow PC (dark beige).

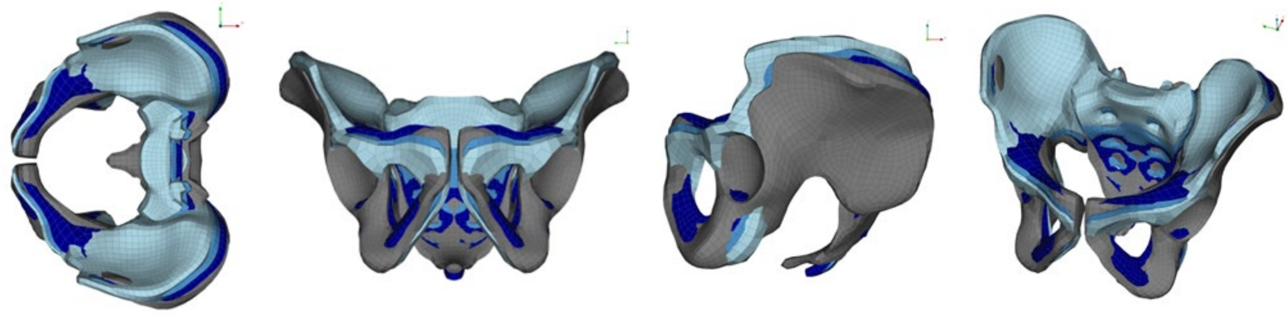

Fig. C-8. Pelvis orientation: THUMS midsize male positioned (gray), HBM-Connect 50M v2.5 pelvis in default position (light blue), after positioning workflow UF (middle blue), after positioning workflow PC (dark blue).

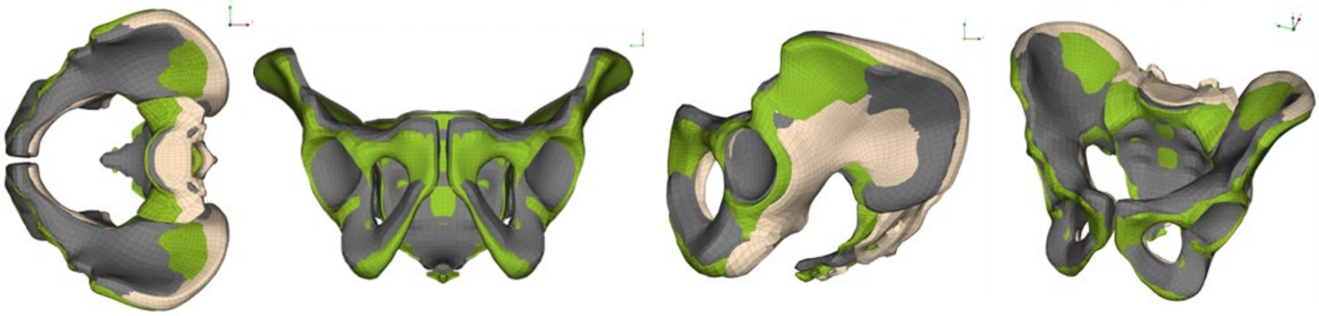

Fig. C-9. Pelvis orientation: THUMS midsize male positioned (gray), VIVA+ 50M v2.0.1 pelvis in default position (light beige) and after positioning workflow PF/TH (green).

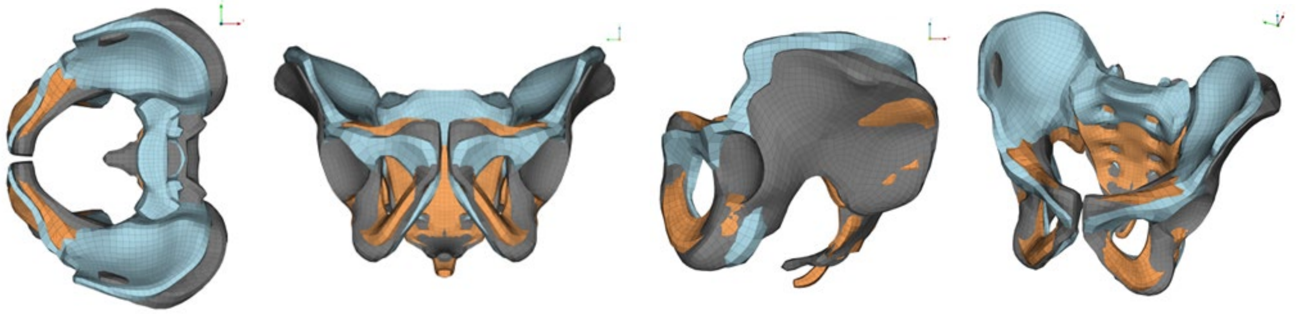

Fig. C-10. Pelvis orientation: THUMS midsize male positioned (gray), HBM-Connect 50M v2.5 pelvis in default position (light blue) and after positioning workflow PF/TH (orange).

D) HBM Coordinate Deviations for each Workflow

Yellow = Landmarks used for WF
White/grey = Specific coordinate wasn't considered in positioning process

	THUMS Target Coordinates			VIVA+ 50M v2.0.1 Coordinates				Deviations		
Landmarks	x	y	z	Node ID	x	y	z	x	y	z
H-Point	834.79898	-3.25E-05	331.94754	6091000	835.40002	0.00	331.5	0.6	0.0	-0.4
Infraorbitale_R	939.9624	34.88775	950.9406	1032018	941.20001	35.299999	950.70001	1.2	0.4	-0.2
Infraorbitale_L	939.9626	-34.88545	950.9404	1013729	941.20001	-35.299999	950.70001	1.2	-0.4	-0.2
HM_R	781.61865	285.88766	645.8359	3629893	789.40002	284.80002	643.90002	7.8	-1.1	-1.9
HM_L	781.61865	-285.88766	645.8359	3129893	789.40002	-284.70001	643.90002	7.8	1.2	-1.9
US_R	545.2263	263.93576	701.3562	3600750	545.20001	263.89999	701.40002	0.0	0.0	0.0
US_L	545.2263	-263.93576	701.3562	3100750	545.20001	-263.89999	701.40002	0.0	0.0	0.0
FE_R	404.4706	148.71729	426.20767	7630319	407.60001	147.7	426.5	3.1	-1.0	0.3
FE_L	403.3925	-169.0787	405.73883	7130319	407.10001	-167.2	406.39999	3.7	1.9	0.7
IM_R	151.196464	137.09631	76.007221	8000000	151.2	137.10001	76	0.0	0.0	0.0
IM_L	129.641517	-203.86911	82.225502	8000001	129.6	-203.9	82.2	0.0	0.0	0.0

Fig. D-1. Coordinate deviations of VIVA+ 50M after workflow UF.

	THUMS Target Coordinates			VIVA+ 50M v2.0.1 Coordinates				Deviations		
Landmarks	x	y	z	Node ID	x	y	z	x	y	z
ASIS-R	859.38	115.62	414.54	6130250	859.79999	115.3	412.10001	0.4	-0.3	-2.4
ASIS-L	859.38	-115.62	414.54	6109901	859.5	-115.8	413.5	0.1	-0.2	-1.0
Pubic_Symphysis	789.8	0.012	366.23	6622026	787.79999	0.5	368.5	-2.0	0.5	2.3

Fig. D-2. Coordinate deviations of VIVA+ 50M after workflow PC.

	THUMS Target Coordinates			VIVA+ 50M v2.0.1 Coordinates				Deviations		
Landmarks	x	y	z	Node ID	x	y	z	x	y	z
H-Point	834.79898	-3.25E-05	331.94754	6091000	834.90002	0.00	331.89999	0.1	0.0	0.0
ASIS-R	859.38	115.62	414.54	6130250	855.10004	114.9	410.89999	-4.3	-0.7	-3.6
ASIS-L	859.38	-115.62	414.54	6109901	854.60004	-117.6	409.89999	-4.8	-2.0	-4.6
Pubic_Symphysis	789.8	0.012	366.23	6622026	785.5	0.00	363.10001	-4.3	0.0	-3.1
HM_R	781.61865	285.88766	645.8359	3629893	789.10004	286.30002	642.90002	7.5	0.4	-2.9
HM_L	781.61865	-285.88766	645.8359	3129893	789.10004	-286.20001	642.90002	7.5	-0.3	-2.9
US_R	545.2263	263.93576	701.3562	3600750	545.20001	263.89999	701.40002	0.0	0.0	0.0
US_L	545.2263	-263.93576	701.3562	3100750	545.20001	-263.89999	701.40002	0.0	0.0	0.0
FE_R	404.4706	148.71729	426.20767	7630319	408.20001	146.5	425.00	3.7	-2.2	-1.2
FE_L	403.3925	-169.0787	405.73883	7130319	407.5	-166.5	406.30002	4.1	2.6	0.6
IM_R	151.196464	137.09631	76.007221	8000000	151.2	137.10001	76.00	0.0	0.0	0.0
IM_L	129.641517	-203.86911	82.225502	8000001	129.60001	-203.90001	82.200005	0.0	0.0	0.0

Fig. D-3. Coordinate deviations of VIVA+ 50M after workflow PF.

	THUMS Target Coordinates			VIVA+ 50M v2.0.1 Coordinates				Deviations		
Landmarks	x	y	z	Node ID	x	y	z	x	y	z
Head COG	1024.3778	0.0366091	984.25525	1090010	1024.4	0.00	984.29999	0.0	0.0	0.0
Acromion_R	1022.2185	186.37244	775.2306	3655787	1024.8	176.2	777.10004	2.6	-10.2	1.9
Acromion_L	1022.2185	-186.37244	775.2306	3155787	1024.9	-176.10001	777.20001	2.7	10.3	2.0

Fig. D-4. Coordinate deviations of VIVA+ 50M after workflow TH.

	THUMS Target Coordinates			HBM-Connect 50M v2.5 Coordinates				Deviations		
Landmarks	x	y	z	Node ID	x	y	z	x	y	z
H-Point	834.79898	-3.25E-05	331.94754	10400001	834.79999	0.0	331.89999	0.0	0.0	0.0
Infraorbitale_R	939.9624	34.88775	950.9406	10010211	938	37.400002	962.20001	-2.0	2.5	11.3
Infraorbitale_L	939.9626	-34.88545	950.9404	10110211	938	-37.400002	962.20001	-2.0	-2.5	11.3
HM_R	781.61865	285.88766	645.8359	10601933	781.90002	285.89999	645.79999	0.3	0.0	0.0
HM_L	781.61865	-285.88766	645.8359	10701933	781.90002	-285.89999	645.79999	0.3	0.0	0.0
US_R	545.2263	263.93576	701.3562	10601587	545.20001	263.89999	701.40002	0.0	0.0	0.0
US_L	545.2263	-263.93576	701.3562	10701587	545.20001	-263.89999	701.40002	0.0	0.0	0.0
FE_R	404.4706	148.71729	426.20767	10617016	403.60001	148.7	426.10001	-0.9	0.0	-0.1
FE_L	403.3925	-169.0787	405.73883	10717016	402.80002	-169.10001	405.70001	-0.6	0.0	0.0
IM_R	151.196464	137.09631	76.007221	10600150	156	137.5	82.300003	4.8	0.4	6.3
IM_L	129.641517	-203.86911	82.225502	10700150	132.8	-203.3	85.400002	3.2	0.6	3.2

Fig. D-5. Coordinate deviations of HBM-Connect 50M after workflow UF.

	THUMS Target Coordinates			HBM-Connect 50M v2.5 Coordinates				Deviations		
Landmarks	x	y	z	Node ID	x	y	z	x	y	z
ASIS-L	859.38	-115.62	414.54	10504352	854.90002	-112.4	412.39999	-4.5	3.2	-2.1
ASIS-R	859.38	115.62	414.54	10404352	855	112.4	412.39999	-4.4	-3.2	-2.1
Pubic_Symphysis	789.8	0.012	366.23	10409406	788.40002	0.0	364	-1.4	0.0	-2.2

Fig. D-6. Coordinate deviations of HBM-Connect 50M after workflow PC.

	THUMS Target Coordinates			HBM-Connect 50M v2.5 Coordinates				Deviations		
Landmarks	x	y	z	Node ID	x	y	z	x	y	z
H-Point	834.79898	-3.25E-05	331.94754	10400001	834.79999	0.0	331.89999	0.0	0.0	0.0
ASIS-L	859.38	-115.62	414.54	10504352	859.0	-110.8	408.39999	-0.4	4.8	-6.1
ASIS-R	859.38	115.62	414.54	10404352	859.0	110.8	408.39999	-0.4	-4.8	-6.1
Pubic_Symphysis	789.8	0.012	366.23	10409406	788.20001	0.0	363.80002	-1.6	0.0	-2.4
HM_R	781.61865	285.88766	645.8359	10601933	781.900024	285.899994	645.799988	0.3	0.0	0.0
HM_L	781.61865	-285.88766	645.8359	10701933	781.900024	-285.89999	645.799988	0.3	0.0	0.0
US_R	545.2263	263.93576	701.3562	10601587	545.200012	263.20001	701.400024	0.0	-0.7	0.0
US_L	545.2263	-263.93576	701.3562	10701587	545.200012	-263.20001	701.400024	0.0	0.7	0.0
FE_R	404.4706	148.71729	426.20767	10617016	402.70001	148.5	426.5	-1.8	-0.2	0.3
FE_L	403.3925	-169.0787	405.73883	10717016	402.0	-169.0	406.0	-1.4	0.1	0.3
IM_R	151.196464	137.09631	76.007221	10600150	155.7	138.7	82.099998	4.5	1.6	6.1
IM_L	129.641517	-203.86911	82.225502	10700150	133.0	-204.3	85.5	3.4	-0.4	3.3

Fig. D-7. Coordinate deviations of HBM-Connect 50M after workflow PF.

	THUMS Target Coordinates			HBM-Connect 50M v2.5 Coordinates				Deviations		
Landmarks	x	y	z	Node ID	x	y	z	x	y	z
Head COG	1024.3778	0.0366091	984.25525	10000085	1024.3	0.0	964.79999	-0.1	0.0	-19.5
Acromion_R	1022.2185	186.37244	775.2306	10203400	1022.2	156.4	775.20001	0.0	-30.0	0.0
Acromion_L	1022.2185	-186.37244	775.2306	10303400	1022.2	-156.4	775.20001	0.0	30.0	0.0

Fig. D-8. Coordinate deviations of HBM-Connect 50M after workflow TH.